Journal of Manufacturing Engineering, June, 2014, Vol. 9, Issue. 2, pp 116-123

EFFECT OF CREVICE FORMERS AND APPLIED TORQUE ON CORROSION BEHAVIOUR OF AISI 304L AUSTENITIC STAINLESS STEEL

***Thiruvikraman C[1], Balasubramanian V[2] and Sridhar K[3]**

[1]Research Scholar, Dept. of Manufacturing Engg., Annamalai University, Annamalainagar, Tamilnadu-608002, India
[2]Professor, Dept. of Manufacturing Engg., Annamalai University, Annamalainagar, Tamilnadu-608002, India
[3]Scientist'F', Marine Materials Department, Naval Materials Research Laboratory (NMRL), Ambernath, Maharashtra- 421501, India

ABSTRACT

Corrosion damage of materials at confined spaces such as gaps and contact areas between parts, under gaskets or seals, inside cracks and seams, spaces filled with deposits and under sludge piles is called crevice corrosion. This has important practical implication in pump, fluid transporting pipes, impeller blades and ship hull applications, for instance, where this phenomenon, in stagnant environments with saline water and in the presence of solid particles, can play an important role in material degradation leading to catastrophic failure. In this study AISI 304L Austenitic Stainless Steel specimens were tested for its corrosion resistance under influence of applied torque with different crevice formers. Corrosion resistance measurement was done using Potentiostat. The effect of crevice formers and applied torque on the base material in artificial seawater environment has been studied. The microstructure of the corroded surface and its hardness were characterized by optical microscope, SEM and Vickers's micro hardness tester. Surface characterization of the damaged surface has also been studied using advanced techniques. Crevice corrosion behavior of base metal increased when SS 304 L crevice formers were used.

Keywords: *SS 304 L, Crevice corrosion, Crevice formers and Corrosion resistance.*

1. Introduction

Subsea blowout preventers (BOP) play an extremely important role in providing safe working conditions for drilling activities in 3000 m ultra-deep water regions. Two redundant multiplex control pods, normally located on the lower marine riser package on the seafloor, are of crucial importance to the performance and reliability of BOP systems. The control pods contain 224 submersible solenoid valves immersed in low-temperature and high-pressure seawater [1]. Stainless steel has high corrosion resistance, high strength, and high durability; thus, it serves as the primary materials of submersible valves. It relies on the stability of a thin chromium oxide film for protection against corrosion; however, under aggressive environmental conditions it suffers from severe localized corrosion, especially crevice corrosion [2]. In a used submersible solenoid valve, severe crevice corrosion is observed in the crevice between the valve shell and the spring sleeve, and slight corrosion is detected in the crevice between the sliding seal components and the fluoroelastomeric (FKM) o - rings. Seawater ingress is recognized as the most common cause of crevice corrosion [3].

In recent years, various electrochemical techniques, such as cyclic potentiodynamic polarization, polarization resistance, potentiostatic test, dynamic electrochemical impedance spectroscopy, and the Tsujikawa–Hisamatsu method, have been used to assess the crevice corrosion process [4–11,23–25,27–29]. The effects of variables, such as temperature, crevice former materials, chemical element, crevice geometries, and solutions, on crevice corrosion have been studied [4–19].

The crevice corrosion of stainless steel has a high breakdown potential at low-temperatures and a low breakdown potential at high temperatures [4]. The polytetrafluoroethylene (PTFE) tape-covered ceramic is the most active crevice former on alloy C-22, whereas PTFE and Kel-F are less active and ceramic crevice formers cause no crevice corrosion. In addition, smoother surfaces create tighter crevices, and correspondingly, more severe crevice corrosion with the same former material [5,6]. AISI 304 stainless steel is susceptible to crevice corrosion, but its susceptibility is not highly affected by the use of Teflon or graphite crevice former, whereas AISI 304 crevice former exhibits a major effect on AISI 304 stainless steel [32].

**Corresponding Author - E- mail: ctvikraman@gmail.com*

The corrosion of metal-to-metal crevices was studied in 0.5 M NaCl, 4 M NaCl, and 4 M MgCl solutions at 95 °C, and the torques applied to the assembly were 0.35 N m and 8.4 N m . Except for those in 304L stainless steel, all other metal-to-metal crevices are less susceptible to crevice corrosion than the corresponding metal-to-PTFE crevices [7,8].

The effects of nitrogen and nickel on the crevice corrosion resistance were studied in different chloride solutions [9–11]. These studies indicate that the increase in nitrogen content improves the crevice corrosion resistance of the alloys by decreasing active dissolution and increasing both passive film stability and the potential at which crevice attack is stable [9]. Ferritic steels containing nickel are more resistant to corrosion than both ferritic steels without nickel and austenitic steels [10].

The geometric scaling factors L/G and L/G were defined to study the effect of crevice geometries on crevice corrosion, where L is either the crevice length or the distance between the crevice mouth and the greatest attack site, and G is the crevice gap. The IR drop mechanism was used to describe the onset of crevice corrosion [12–16]. Comparative research on crevice corrosion in different solutions shows that more ethylene glycol makes artificial seawater more corrosive to 316L stainless steel [17–18]. Crevice corrosion can even be initiated and propagated under galvanostatic conditions in an alkaline chloride solution of low Cl /OH ratio [19].

This work aims to investigate the effects of applied torque and crevice former materials on the corrosion behaviour of 304L stainless steel. Three crevices, namely, 304L-to-PTFE, 304L-to-FKM, and 304L-to-304L, were used. The breakdown potential, repassivation potential, corroded surface area, and maximum penetration depth were investigated as a function of applied torque.

2. Experimental Details

The chemical composition of 304L stainless steel used in this research is given in Table 1. A multiple crevice assembly (MCA) based on the standard guide for crevice corrosion testing, ASTM G48 and G78 [20, 21], was used. The base metal microstructure is shown in (Fig. 1(a)). The MCA specimens (50.8 mm x 25.4 mm x 5 mm with a 10 mm diameter hole) were cut from 5 mm thick commercial plates (Fig. 1(b)). Electrical connection to the specimens was established via an isolated Cu wire. The modified crevice formers shown in Fig. 1(c) Twelve crevice sites were made in PTFE, FKM, and 304L stainless steel respectively. Before the crevice corrosion test, all the tested specimens and the teeth of the formers were abraded with wet 800 grit SiC paper, degreased with acetone followed by alcohol, and then air dried. The specimen assembly, which includes a 304L stainless steel specimen and two crevice formers, was tightened with a titanium bolt, nut, and washer using a torque wrench [21], so that 12 small crevice sites were formed on each side of the specimen. PTFE tape was used to insulate the bolt to prevent electrical connection between the titanium bolt and the 304L stainless steel specimen.

The crevice corrosion test was performed in artificial seawater prepared with deionised water and sea salt, the detailed composition of the solution is given in Table 2 [22]. The temperature in 3000 m ultra-deep seawater is about 4 C; thus, the corrosion rate is very low. According to Arrhenius kinetics, a 10°C rise in temperature doubles the reaction rate [3]. I n this study, tests were conducted at 50°C t o accelerate crevice corrosion.

The standard three-electrode cyclic potentiodynamic polarization method was employed according to ASTM G61 [31]. The test cell is schematically shown in Fig. 2. The test cell was composed of a reference electrode (saturated calomel electrode), a counter electrode (silver rod) and a working electrode (stainless steel specimen assembly). In the cyclic potentiodynamic polarization test, a scan was initiated 1 h after the specimen was immersed i n the solution. The scan was initiated from 100 mV below the open circuit potential (OCP) and reversed when the potential reached 200 mV. When the potential reached 100 mV below OCP, the scan was discontinued. The scan rate was 0.167 mV/s in both the forward and reverse scans, and each cyclic potentiodynamic polarization test lasted 3–4 h. A Potentiostat/Galvanostat Model V5 (Gill AC, England) was used to perform the cyclic potentiodynamic polarization test.

After the crevice corrosion experiments, the corroded surface area was calculated using CAD software, and the penetration depth was measured using a dial guage.

Table 1: Chemical compositions (wt %) of SS 304 L

C	Mn	P	S	Si	Cr	Ni	Fe
0.017	1.81	0.025	0.04	0.22	18.59	8.66	Bal

Table 2: Composition of the artificial sea water (g/L)

NaCl	$MgCl_2$	Na_2SO_4	$CaCl_2$	$NaHCO_3$	KBr	H_3BO_3
24.53	5.2	4.09	1.16	0.201	0.10	0.027

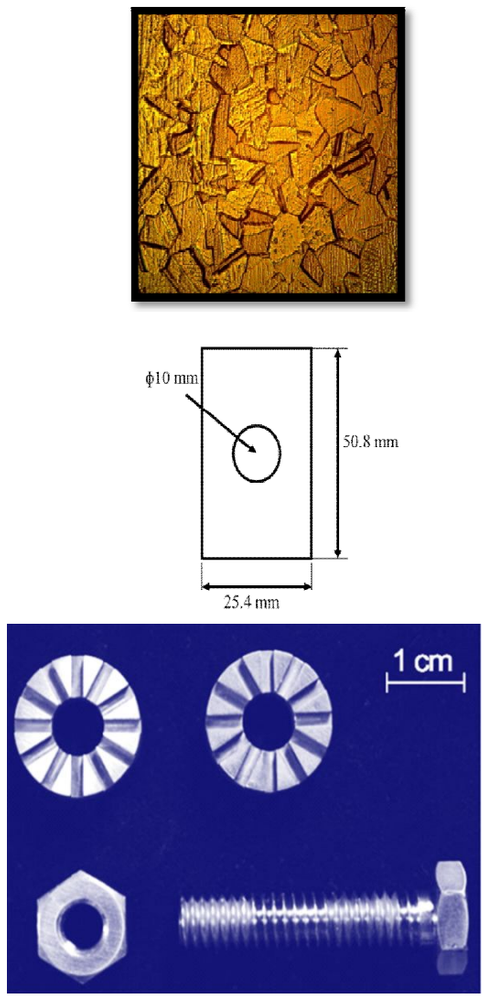

Fig. 1 Multiple Crevice Assembly (MCA) (a) base material microstructure (b) dimensions of MCA specimen; (c) 304L crevice former with crevice sites.

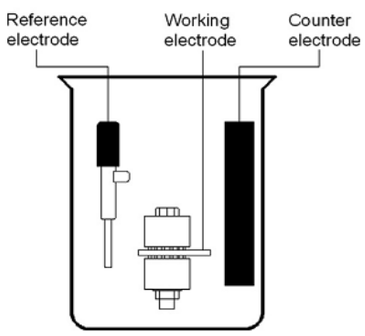

Fig. 2 Schematic diagram of the three-electrode test cell

3. Results and Discussion

3.1 Cyclic Potentiodynamic Polarization Curves

Fig. 3(a) and (b) show the cyclic potentiodynamic polarization results of the 304 L stainless steel specimens assembled with 304 L stainless steel former and PTFE former under the same applied torques of 4 Nm in artificial seawater at 50 °C.

In the cyclic potentiodynamic polarization curve, four typical potentials, namely, corrosion potential (E_{corr}), primary passivation potential (E_{pp}), breakdown potential (E_b) and repassivation potential (E_{rp}) are usually used to characterise the crevice corrosion behaviour. Corrosion potential also called OCP, is the electrical potential between the working electrode and the reference electrode when no electrical current flows. As shown in Fig. 3(a) and (b), both of the measured E_{corr} values are approximately - 330 mV_{SCE}. The values are similar to those of 304L-to-304L, 304L-to-PTFE and 304L-to-FKM crevice corrosion tested at any applied torque in artificial seawater at 50°C. The value of the primary passivation potential is not obvious in the cyclic potentiodynamic polarization curve. The estimated primary passivation potentials are given in Fig. 3(a) and (b).

In breakdown potential, current density increases significantly and rather rapidly. The more noble the potential obtained at a fixed scan rate, the less susceptible the alloy is to the initiation of localized corrosion (pitting and crevice corrosion) [31]. In cyclic potentiodynamic polarization tests, crevice corrosion occurs more easily than pitting because the occurrence of pitting corrosion requires higher electrochemical potentials [8, 19, and 30]. Breakdown potential has several definitions [23, 25]. It is determined by the extrapolation of passive current and ascending current in reference [23]. In this study, the value at the turning point of the curve is considered the breakdown potential. As shown in Fig. 3(a) and (b), the measured breakdown potential of 304L-to-304L crevice corrosion is -15 mV_{SCE}. This value is slightly lower than that of 304L-to-PTFE crevice corrosion, which has an E_b value of 10 mV_{SCE}. When the potential drops to a specific value on the reverse scan, the current decreases to the level of passive current, and the potential is referred to as repassivation potential. The more electropositive the potential, the less likely that localized corrosion occurs [31]. Repassivation potential also has several definitions [7, 25, 31]. In reference [7], the repassivation potential is defined as the potential at which the current density remains below 2 $x10^{-6}$ Acm^{-2} on the reverse scan,

whereas reference [25] defines it as the potential at which the reverse and forward scans intersect or at which the current density reaches 2 x10^{-6} Acm^{-2} on the reverse scan. However, in this study, the current density is always greater than 2 x10^{-6} Acm^{-2} on the reverse scan, as shown in Fig. 3(a) and (b). In a certain curve, the forward and reverse scans intersect three times, as shown in Fig. 3(b). Therefore, in this study, the repassivation potential is defined as the potential at which the reverse and forward scans intersect for the first time. The E_{rp} value of 304L-to-304L crevice corrosion is -380 mV_{SCE} (Fig. 3(a)). As for 304L-to-PTFE crevice corrosion, the E_{rp} value is - 240 mV_{SCE} , which is the value of the first intersection of the forward and reverse scans, as shown in Fig. 3(b).

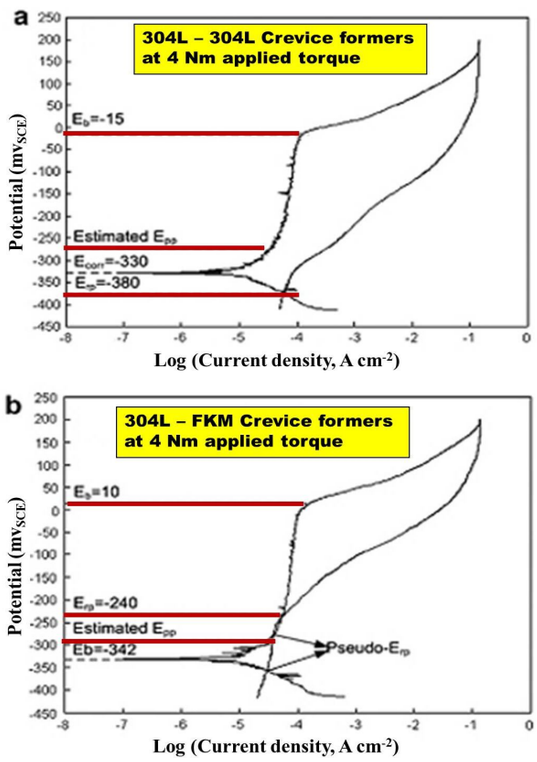

Fig. 3: Cyclic potentiodynamic polarization curves of (a) 304L-to-304L; (b) 304L-to-PTFE crevice corrosion at 4 Nm applied torque in artificial seawater.

Crevice corrosion is normally considered to occur if the corrosion potential of a metal in a given environment exceeds the repassivation potential [7, 28]. For 304L-to-304L crevice corrosion at 4 Nm applied torque, crevice corrosion can begin because the Ecorr value of - 330 mVSCE is higher than the Erp value of -380 mVSCE. Visual observation of the specimens after the experiments indicates that crevice corrosion occurs on both sides of the 304L stainless steel specimen, and all the 24 crevice sites are aggressively attacked. For 304L-to-PTFE crevice corrosion at 4 N m applied torque, because the E_{corr} value of -332 mV_{SCE} is lower than the E_{rp} value of -240 mV_{SCE} , crevice corrosion cannot initiate. No crevice corrosion is observed on the 304L stainless steel specimen after being coupled to PTFE crevice former.

3.2. Effects of applied torque on breakdown potential and repassivation potential

Crevice corrosion breakdown potential and repassivation potential are the two most important electrochemical parameters in the cyclic potentiodynamic polarization curve. The E_b value, E_{rp} value and their difference ($\Delta E = E_b - E_{rp}$) were measured to determine crevice corrosion susceptibility. Fig. 4 (a–c) summarise the E_b , E_{rp} , and ΔE values of 304L stainless steel obtained over a wide range of applied torques when PTFE, FKM, and 304L stainless steel were used as the crevice former materials in artificial seawater at 50°C.

As shown in Fig. 4(a), for 304L-to-PTFE crevice corrosion, when the applied torque is 0.02 Nm, the E_b and E_{rp} values are high, and the E_{rp} value of -280 mV_{SCE} is greater than the E_{corr} value of -326 mV_{SCE} . This implies that no crevice corrosion occurs. The examination result of the 304L stainless steel specimen confirms the absence of corrosion.

When the applied torque is higher than 0.2 N m , the E_b reaches a stable level of approximately 10 mV_{SCE} , and the E_{rp} reaches a stable level of approximately -380 mV_{SCE}. The stable values of applied torque are appropriate for maintaining the critical conditions for crevice corrosion initiation and propagation, so that crevice corrosion on specimens can be observed. Similar results were reported in literature [26–28]. When the applied torque is higher than 0.98 N m , the repassivation potential of 304 stainless steel in NaCl solution using polysulfone gaskets at 55°C becomes stable [26]. The same tendency is displayed for Alloy 22 PCA specimens tested in 1 M NaCl solution with PTFE tape-covered ceramic crevice former. However, i n this case, the E_{rp} become stable at a torque higher than 3.4 N m in 1 M NaCl at 90°C [27, 28]. In this study, when the applied torque is greater than 2 N m, the E_b value is unchanged, whereas the E value rapidly increases. This observation has not been previously reported. Less corrosion is observed at the edges of the crevice sites when the

applied torque is 3 Nm. No corrosion is detected at an applied torque of 4 Nm, even. The stable values of ΔE at torques from 0.2 to 2 Nm are higher than those at any other applied torques. Therefore, it can be inferred that the higher the ΔE, the more susceptible the metal is to the initiation of crevice corrosion, which agrees with the results in reference [28]. The examination result shows that crevice corrosion occurs on both sides of the 304L stainless steel specimens at torques from 0.2 to 2 Nm. Similar curves are displayed for 304L-to-FKM crevice corrosion. As shown in Fig. 4(b), when the applied torque is higher than 0.01 Nm, the E_b value is stable up to approximately 30 mV_{SCE} , and the E_{rp} value is approximately -360 mV_{SCE}. The E_{rp} value again becomes higher if the applied torque is greater than 0.1 Nm, which is similar to observations on 304L-to-PTFE crevice corrosion.

As shown in Fig. 4(c), for 304L-to-304L crevice corrosion, the values change slightly with increasing applied torque. The turning point of the applied torques is 5 Nm, and the stable values of E_b, E_{rp} and ΔE are -15 mV_{SCE}, - 400 mV_{SCE} , and 385 mV_{SCE} , respectively. After comparing Fig. 4(a–c), it can be seen that the relationship of the stable values of E_b, E_{rp} , and ΔE are $E_{b(304L)} < E_{b(PTFE)} < E_{b(FKM)}$, $E_{rp(304L)} < E_{rp(PTFE)} < E_{rp(FKM)}$, and $\Delta E_{b(304L)} \approx \Delta E_{b(PTFE)} \approx \Delta E_{b(FKM)}$, respectively, showing that the 304L-to-304L crevice shows the highest susceptibility to crevice corrosion, whereas the 304L-toFKM crevice shows the lowest susceptibility. This indicates that FKM is more effective in preventing water from penetrating into crevices. The high performance of FKM against crevice corrosion of 304L stainless steel stems from its hydrophobic property [33]. Similar results were reported for silicone-to-444 stainless steel crevice corrosion [34].

3.4. Corrosion Morphology

The crevice-corroded 304L stainless steel specimen, after being coupled to 304L stainless steel crevice former at 10 N m applied torque in artificial seawater is shown in Fig. 5(a-c). The image shows that all the 12 crevice sites are attacked for 304L – 304L. For further examination, a single site is magnified, as shown in Fig. 5(c). The corrosion regions are schematically drawn in lines (Fig. 5(d)).

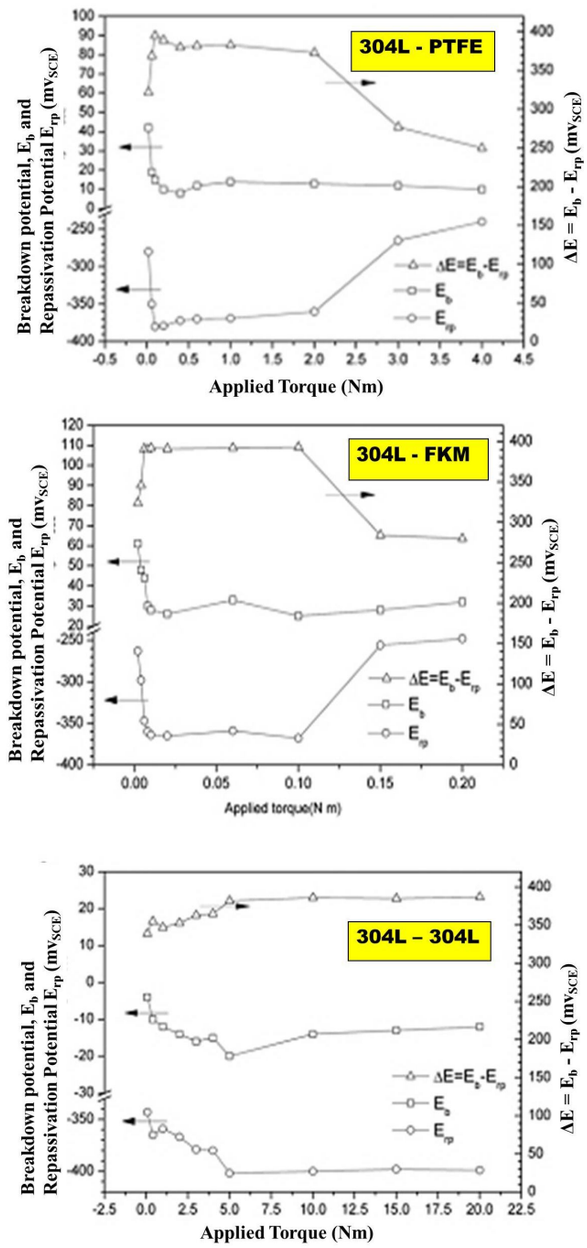

Fig. 4: Measured breakdown potentials, repassivation potentials and ΔE as a function of applied torques of (a) 304L-to-PTFE; (b)304L -to-FKM; and (c) 304L-to-304L crevice corrosion in artificial seawater.

At the corrosion surface, three regions extending from the boundary of the tooth to the centre inside the crevice can be observed: (A) passive region, (B) active region, and (C) variable region. Similar morphology was reported for crevice corrosion in nickel [12] and iron [16]. The active region consists of three sub-regions: (1) severely attacked region, (2) commonly attacked region and (3) lightly attacked region.

As shown in Fig. 5(c), the passive region is observed from the edge of the crevice to a critical distance inside the crevice (termed x_{crit}). In the passive region, the metal suffers from less attack. Crevice corrosion occurs at the passive-to-active boundary, x_{cirt}, where the IR drop equals $\Delta\phi$, which is defined as the difference between the outer surface potential and the passivation potential [35].

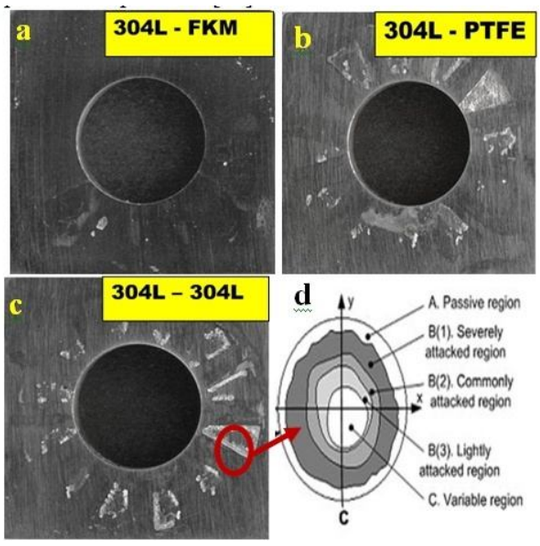

Fig. 5. Crevice-corroded specimens after being coupled to 304L stainless steel in artificial seawater. (a) 304L - FKM (b) 304L - FKM (c) 304L - 304L (d) regions of the single crevice corrosion site.

In the active region, the metal which has an extremely rough surface, suffers from severe attack. The crevice potential decreases with decreasing x_{cirt} (deeper into the crevice); thus, the active region can be further subdivided into three small regions. In the severely attacked region, the metal dissolves severely and assumes the shapes of furrows (Fig. 6). The commonly attacked region is lightly desquamated. The first two regions present the natural colour of stainless steel. The lightly attacked region is dark due to the existence of residual corrosion products on the corroded surface. The variable region is located at the centre of the crevice tooth, where both passive and active attacks are observed.

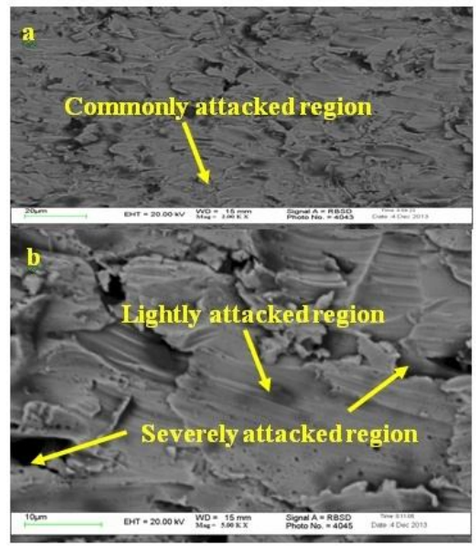

Fig. 6: SEM micrographs of different regions of the 304L-to-304L crevice site at 10 N m applied torque in artificial sea water region

4. Conclusions

(1) The influence of applied torque on breakdown potential, repassivation potential, corroded surface area, and maximum penetration depth are similar and obvious for 304L-to-PTFE and 304L-to-FKM corrosion. However, the influence is insignificant for 304L-to-304L crevice corrosion.

(2) 304L-to-304L crevice corrosion has the lowest stable values of breakdown potential and repassivation potential, whereas 304L-to-FKM crevice corrosion shows the highest, indicating that among the three crevices, 304L-to-304L crevice is the most susceptible t o crevice corrosion, whereas 304L-toFKM crevice is the least susceptible.

(3) 304L-to-304L crevice corrosion exhibits a maximum corroded surface area and a maximum penetration depth, followed by those of 304L-to-PTFE crevice corrosion. 304L-to-FKM crevice corrosion exhibits a minimum corroded surface area and a minimum penetration depth.

(4) Three regions, namely, the passive, active (consisting of severely attacked, commonly attacked and lightly attacked regions) and variable regions, can be observed on most crevice corrosion sites.

Acknowledgments

The authors wish to express their sincere thanks to the Materials Panel, Naval Research Board (NRB), Ministry of Defense, Govt. of India, New Delhi for the financial support extended to carry out this investigation through the sponsored project No DNRD/05/4003/NRB/212 . The authors wish to place their sincere thanks on record to The Director, Naval Materials Research Laboratory (NMRL), Ambernath for extending facilities to characterize the coatings.

References

1. *Shaughnessy J M and Armagost W K (1999), "Problems of Ultra-Deepwater Drilling", 1999 SPE/IADC Drilling Conference, Holland, 9, SPE/IADC 52782.*
2. *Fossati A, Borgioli F, Galvanetto E and Bacci T (2006),"Corrosion resistance properties of glow-discharge nitrided AISI 316L austenitic stainless steel in NaCl solutions", Corros. Sci. Vol.48, 1513–1527.*
3. *Turner P A (2001), "Material Compatibility in Directional Control Valve Designs", Offshore Technology Conference, Houston, OTC13233.*
4. *Jakobsen P T and Maahn E (2001), "Temperature and potential dependence of crevice corrosion of AISI316 stainless steel", Corros. Sci. Vol. 43, 1693–1709.*
5. *Shan X and Payer J H (2007), "Comparison of Ceramic and Polymer Crevice Formers on the Crevice Corrosion Behavior of Ni–Cr–Mo Alloy C-22, Corrosion/07", NACE International, Nashville, TN, 07582.*
6. *Shan X and Payer J H (2008),"Effect of Crevice Former on the Evolution of Crevice Damage", Corrosion/08, NACE International, New Orleans, LO, 08575.*
7. *He X, Dunn D S and Csontos A A (2007), "Corrosion of similar and dissimilar metal crevices in the engineered barrier system of a potential nuclear waste repository", Electrochim. Acta 52 7556–7569.*
8. *He X and Mintz T(2008),"Localized Corrosion of Alloy 22 in the potential yucca mountain repository environment", JOM 60 44–51.*
9. *Mudali U K and Dayal R K (2000), "Influence of nitrogen addition on the crevice corrosion resistance of nitrogen-bearing austenitic stainless steels", J. Mater. Sci, Vol.35 ,1799–1803.*
10. *Azuma S, Kudo T, Miyuki H, Yamashita M and Uchida H (2004), Effect of nickel alloying on crevice corrosion resistance of stainless steels, Corros. Sci. Vol. 46 ,2265–2280.*
11. *Baba H and Katada Y (2006), "Effect of nitrogen on crevice corrosion in austenitic stainless steel", Corros. Sci. Vol 48, 2510–2524.*
12. *Lee J S, Reed M L and Kelly R G (2004), "Combining rigorously controlled crevice geometry and computational modeling for study of crevice corrosion scaling factors", J. Electrochem. Soc., Vol. 151, B423–B433.*
13. *Heppner K L, Evitts R W and Postlethwaite J (2004), "Effect of the crevice gap on the initiation of crevice corrosion in passive metals", Corrosion, Vol. 60, 718–728.*
14. *Vankeerberqhen M(2004), Critical characteristic dimension or geometry for determining the susceptibility of a crevice to crevice corrosion, Corrosion, Vol. 60, 707–717.*
15. *Pickering H W (2003), Important early developments and current understanding of the IR mechanism of localized corrosion, J. Electrochem. Soc. Vol. 150, K1–K13.*
16. *Abdulsalam M I (2005), Behaviour of crevice corrosion in iron, Corros. Sci.Vol. 47, 1336–1351.*
17. *Zheng L, Neville A, Andrew G and David J (2008),"Investigation into the Corrosion Behavior of Stainless Steel 316L in Hydraulic Fluids for Subsea Applications", Corrosion/08, NACE International, New Orleans, LO, 08236.*
18. *Zheng L, Neville A, Andrew G and David J (2010), "An experimental study of the corrosion behavior of nickel tungsten carbide in some water–glycol hydraulic fluids for subsea applications", J. Mater. Eng. Perform, Vol. 19 90–98.*
19. *Wang S, Newman R C (2004), Crevice corrosion of type 316Lstainless steel in alkaline chloride solutions, Corrosion, Vol. 60, 448–454.*
20. *ASTM Standard G48, Standard Test Methods for Pitting and Crevice Corrosion Resistance of Stainless Steels and Related Alloys by Use of Ferric Chloride Solution, 2003.*
21. *ASTM Standard G78, Standard Guide for Crevice Corrosion Testing of Iron-Base and Nickel-Base Stainless Alloy in Seawater and Other Chloride-Containing Aqueous Environments, 2007.*
22. *Gerengi H, Darowicki K, Bereket G, Slepski P (2009), "Evaluation of corrosion inhibition of brass-118 in artificial seawater by benzotriazole using dynamic EIS", Corros. Sci., Vol. 51 2573–2579.*
23. *Shan X, Ha H, Payer J H (2009), Comparison of crevice corrosion of Fe-based amorphous metal and crystalline Ni–Cr–Mo Alloy, Metall. Mat. Trans. A: Phys. Metall. Mat. Sci., Vol. 40 1324–1333.*
24. *Nagarajan S, Rajendran N (2009), "Crevice corrosion behaviour of superaustenitic stainless steels: dynamic electrochemical impedance spectroscopy and atomic force microscopy studies", Corros. Sci,. 51217–224.*
25. *Evabs K J, Yilmaz A, Day S D (2005), "Using electrochemical methods to determine alloy 22's crevice corrosion repassivation potential", JOM, vol. 57, 56–61.*
26. *Akashi M, Nakayama G, Fukuda T, "Initiation Criteria for Crevice Corrosion of Titanium Alloys Used for HLW Disposal Overpack", Corrosion/98, NACE International, San Diego, Ca, 1998 (Paper No. 98158).*
27. *Evans K J, Rebak R B (2007), "Measuring the repassivation potential of alloy 22 using the potentiodynamic–galvanostatic–potentiostatic method", J. ASTM Int. 4 (Paper ID JAI101230).*
28. *Carranza R M (2008), "the crevice corrosion of alloy 22 in the Yucca mountain nuclear waste repository", JOM, Vol. 60, 58–65.*
29. *Rebak R B (2009), "Stifling of crevice corrosion in alloy 22 during constant potential tests", J. Pressure Vessel Technol. 131 1–7.*

30. *Tait W S (1994), "An Introduction to Electrochemical Corrosion Testing for Practicing Engineers and Scientists", Wisconsin: Pairodacs Publications, pp. 26–28.*

31. *ASTM Standard G 61, Standard Test Method for Conducting Cyclic Potentiodynamic Polarization Measurements for Localized Corrosion Susceptibility of Iron-, Nickel-, or Cobalt-Based Alloys, 2009.*

32. *Mele G, Bozzini B (2010), "Localised corrosion processes of austenitic stainless steel bipolar plates for polymer electrolyte membrane fuel cells", J. Power Sources, 195, 3590–3596.*

33. *Park C J, Lee Y H (2004), "Initiation and repassivation of crevice corrosion of Type 444 stainless steel in chloride solution", Met. Mater. Int., 10, 447–451.*

34. *Chen S, Yan W C, Chen L, Chen Y J, Xu N P (2006), "Morphology and microstructure of core-shell hybrid latexes containing fluoropolymer and acrylic copolymer", Colloid. Polym. Sci., 284 413–421.*

35. *Abdulsalam M I, Pickering H W (1999), "Effect of the applied potential on the potential and current distributions within crevices in pure nickel", Corros. Sci., Vol. 41, 351–372.*

